Geophysical Research Letters

RESEARCH LETTER
10.1029/2021GL092663

Key Points:

- The lunar sinuous rille Rima Sharp is associated with the mare unit sampled by Chang'e-5, and may have emplaced the unit
- Rima Sharp is actually formed by two rilles, ~320 km long Rima Sharp and ~150 long km Rima Mairan, that meet in the middle of the unit
- Rima Sharp formed first, emplacing most of the lava forming the young basalt unit, followed closely by Rima Mairan, embaying Rima Sharp

Supporting Information:

Supporting Information may be found in the online version of this article.

Correspondence to:

L. Xiao and J. W. Head,
longxiao@cug.edu.cn;
James_Head@brown.edu

Citation:

Qian, Y., Xiao, L., Head, J. W., & Wilson, L. (2021). The long sinuous rille system in Northern Oceanus Procellarum and its relation to the Chang'e-5 returned samples. *Geophysical Research Letters*, *48*, e2021GL092663. https://doi.org/10.1029/2021GL092663

Received 24 JAN 2021
Accepted 30 APR 2021

The Long Sinuous Rille System in Northern Oceanus Procellarum and Its Relation to the Chang'e-5 Returned Samples

Yuqi Qian[1,2], Long Xiao[1,2], James W. Head[3], and Lionel Wilson[4]

[1]State Key Laboratory of Geological Processess and Mineral Resources, Planetary Science Institute, School of Earth Sciences, China University of Geosciences, Wuhan, China, [2]Center for Excellence in Comparative Planetology, Chinese Academy of Sciences, Hefei, China, [3]Department of Earth, Environmental, and Planetary Sciences, Brown University, Providence, RI, USA, [4]Lancaster Environment Centre, Lancaster University, Lancaster, UK

Abstract China's Chang'e-5 (CE-5) mission recently returned samples from a young intermediate-Ti mare unit (Em4/P58, ~1.5 Ga) in Northern Oceanus Procellarum. Rima Sharp, previously mapped as the longest lunar sinuous rille, is the most prominent volcanic feature associated with the landing region. Our analysis shows that Rima Sharp is not a single rille, but instead is composed of two separate rilles (Rima Sharp, originating from the North Vent, and Rima Mairan from the South Vent), meeting at ~40.40°N, 48.38°W. Both vent have characteristics suggesting relatively low magma volatile contents. Rima Mairan and associated lavas (southeast of Em4/P58), embay and are slightly younger than Rima Sharp. Rille formation is largely influenced by pre-existing topography (earlier mare surface, proto-wrinkle ridges, highlands); rilles and deposits experienced post-formation deformation (wrinkle ridges, mare subsidence). CE-5 samples probably originate mainly from Rima Sharp's source vent, but may represent deposits from both rilles.

Plain Language Summary A major unanswered question in lunar science is the age and nature of the youngest lunar lava flows, located in the northwest nearside of the Moon but unsampled by Apollo or Luna missions. How long did internal activity and eruption of lavas continue on the Moon? Also very poorly known is the impact flux in the last third of Solar System history. Craters counted on a geologically young lava flow radiometrically dated in the laboratory would answer this question. China's Chang'e-5 (CE-5) mission recently returned samples from just such a young mare unit. But how was this unit emplaced and how does this help us understand the nature of the lava source regions? Rima Sharp, previously thought to be the longest lunar sinuous rille, crosses the young unit. We find that Rima Sharp is actually formed by two rilles, the 320 km-long Rima Sharp and the 150 km-long Rima Mairan, that meet in the middle of the unit. Detailed analysis shows that Rima Sharp was first, forming most of the young basalt unit, followed closely by Rima Mairan, embaying Rima Sharp. Samples returned by CE-5 are most likely to be from the Rima Sharp eruption.

1. Introduction

On December 1, 2020, China's first lunar sample return mission, Chang'e-5 (CE-5), landed at 43.06°N, 51.92°W (Wang et al., 2021) in Northern Oceanus Procellarum, ~170 km northeast of Mons Rümker (Figure 1a), within the Procellarum-KREEP-Terrain (Jolliff et al., 2000). Rima Sharp, the longest lunar sinuous rille (~566 km; Hurwitz et al., 2013) extends across the eastern part of the landing region, approaching within ~15 km of the landing site (Figure 1a).

Northern Oceanus Procellarum was selected as the CE-5 landing site because it contains some of the youngest mare basalts (Liu et al., 2021). Sampling these young flows could profoundly improve our understanding of lunar thermal and impact history (Qian, Xiao, Head, et al., 2021). Em3 and Em4/P58 are two Eratosthenian-aged mare units in the landing region (Figure S1), as mapped by Qian et al. (2018) and Hiesinger et al. (2011) according to composition and chronologies. The area of Em4/P58 (~37,000 km^2), and its mean thickness (~50 m), yield a total volume of ~1,450–2,350 km^3 (Qian, Xiao, Head, et al., 2021).

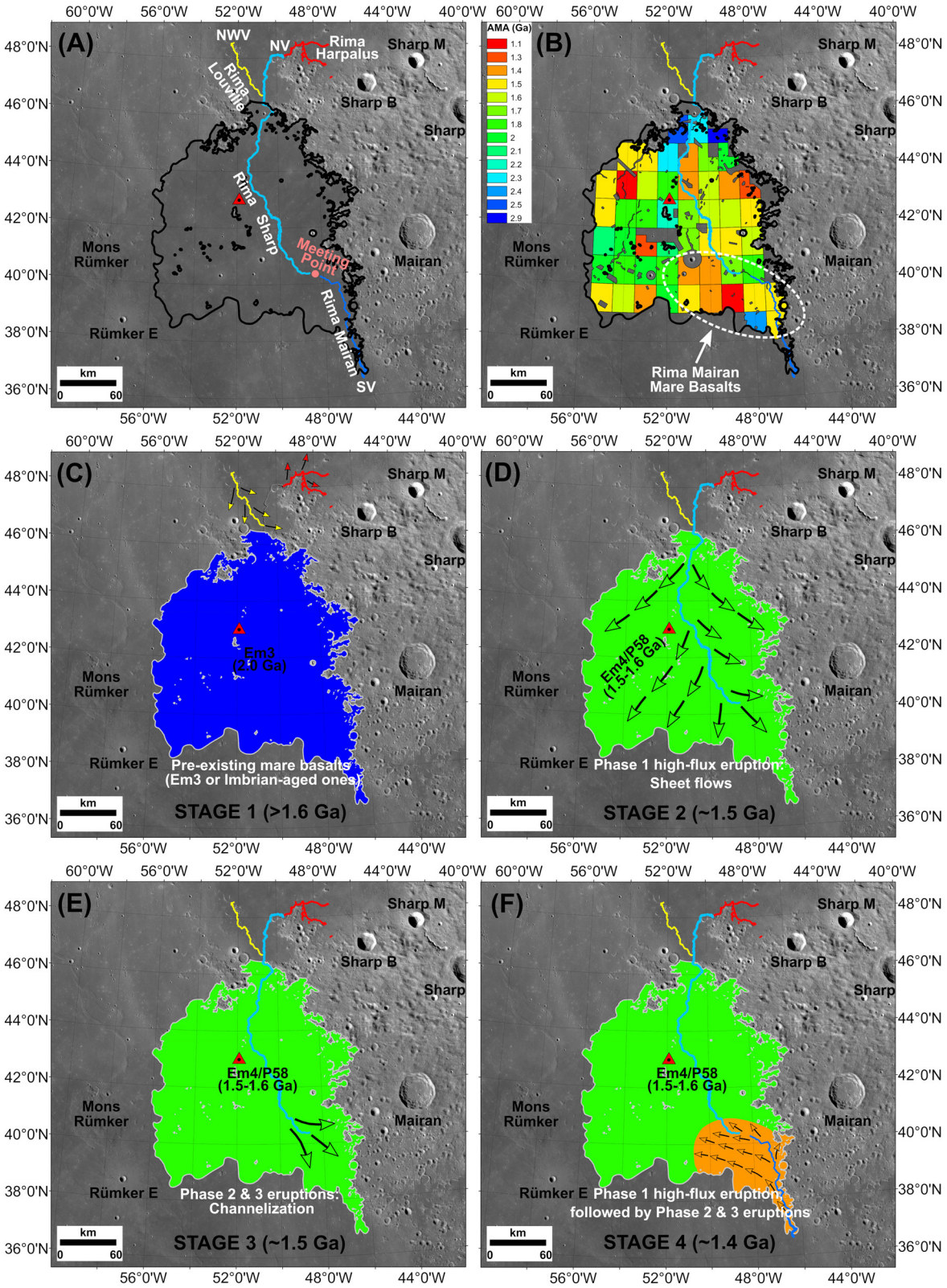

Figure 1. (a) Sinuous rilles across Em4/P58 (black line) in Northern Oceanus Procellarum. The red triangle indicates the CE-5 landing site. (b) Absolute model ages of Em4/P58 (Qian, Xiao, Head, et al., 2021). (c–f) The geological evolution of Em4/P58. (c) Em3 or Imbrian-aged mare basalts covered the current Em4/P58 mare region before its eruption. (d–e) Phase 1 high-flux eruption produced sheet flows, followed by Phase 2/3 channelization (green). (f) The eruption of Rima Mairan produced lavas covering the southeast of Em4/P58 (brown).

For any sample return mission, it is critical to understand the provenance of samples to be able to fully address the scientific objectives through laboratory studies. Therefore, unraveling the source of the young mare basalts is critical to sample interpretations. The CE-5 landing site is covered mainly by local basaltic regolith (~91 wt.%), and minorly by exotic materials from Harpalus, Copernicus and Aristarchus craters (Qian, Xiao, Wang, et al., 2021). There are no eruption fissures within Em4/P58 (Qian, Xiao, Head, et al., 2021), except for Rima Sharp, making it the most probable local source of the returned samples.

For Rima Prinz, an ~87 km long, ~1.1 km-wide, and ~170 m-deep sinuous rille east of the Aristarchus Plateau, its formation to require ~50–250 km^3 of lavas (Hurwitz et al., 2012). Could ~1,450–2,350 km^3 of lava have been delivered by the much longer Rima Sharp (~566 km) to form Em4/P58? If so, what can we learn about eruption conditions and petrogenesis from the source vent, associated deposits, morphology, and mode of emplacement of Rima Sharp? Based on these questions, we conducted a comprehensive study of the nature, origin, and evolution of Rima Sharp (a) to determine the contribution of sinuous rilles to the CE-5 samples, (b) to increase our understanding of the source(s) and petrogenesis of the young basalts, and (c) to deepen our knowledge of the formation and evolution of sinuous rilles.

2. Characterization of Sinuous Rilles

Sinuous rilles are elongated, meandering channels that occur primarily in the lunar maria, and often begin at circular, elongated, or arcuate depressions interpreted to be source vents, often with associated pyroclastic deposits (Head & Wilson, 2017). Somewhat similar in planform to smaller lava channels, sinuous rilles are typically longer, wider, and deeper than such features and can form in the highlands, with little evidence of flanking levees commonly associated with lava channels, before extending into the maria (Oberbeck et al., 1971). For these reasons, it has been proposed that rilles are related to extrusive lava flows in origin, but owe their large length, width, and depth to processes of thermo-mechanical erosion of the substrate (Carr, 1974; Hulme, 1973), with some contributions from both construction and erosion (Roberts & Gregg, 2019).

In a global study, Hurwitz et al. (2013) compiled a catalog of more than 200 rille locations and characteristics. As a population, these vary in length (2–566 km; median 33.2 km), width (0.16–4.3 km; median 480 m), depth (4.8–534 m; median 49 m), slope (1.41°–0.51°; median 0.21°), and sinuosity index (1.02–2.1; median 1.19). The highest concentration of mapped rilles (48%) occurs in the Procellarum-KREEP-Terrain.

Rima Sharp associated with the CE-5 landing site was originally regarded as one single rille (Hurwitz et al., 2013). However, our detailed geomorphologic investigations show that Rima Sharp is actually composed of four independent rilles, that is, Rima Mairan, Rima Sharp, Rima Harpalus, and Rima Louville (unofficial names based on the nearest IAU-named feature; Figure 1a). Three independent source vents have been recognized to the north, northwest, and south of Em4/P58, labeled as North Vent (NV), Northwest Vent (NWV), and South Vent (SV), respectively. Sinuous rilles originate from these three vents, and generally follow regional slope, extending into the young mare unit (Figure S2). In this study, we assess these rilles and their relation to Em4/P58. Morphology analysis are based on Kaguya Terrain Camera (TC) Morning Map (Haruyama et al., 2008) and Lunar Reconnaissance Orbiter NAC/WAC data (Robinson et al., 2010). All elevation estimations are based on SLDEM2015 (~60 m/pixel, Barker et al., 2016); TiO_2 abundance data are from Sato et al. (2017) and the false-color map is based on Kaguya MI data (Kodama et al., 2010).

2.1. Rima Mairan

Rima Mairan originates from SV close to the silica-rich Mairan domes **(**Figure 2a**)**. SV is composed of four circular depressions (Figures 3a–3c), that is, SV1, SV2, SV3, and SV4. SV1 (~560 m-wide, ~255 m-deep) and SV2 (~740 m-wide, ~265 m-deep) form a linear depression (~3,190 m-long, SE-NW); and SV3 (900 m-wide and 265 m-deep) and SV4 (740 m-wide and 144 m-deep) form another linear vent (SW-NE). SV1/SV2 are located outside Em4/P58, while SV3/SV4 are inside. SV3/SV4 appear more disrupted while SV1/SV2 are contiguous. Both SV3 and SV4 are rimless, indicating that they are not impact features (Figure 3b). The western edges of SV3/SV4 are in the center of the rille channel, lower than the mare surface but higher than the rille floor.

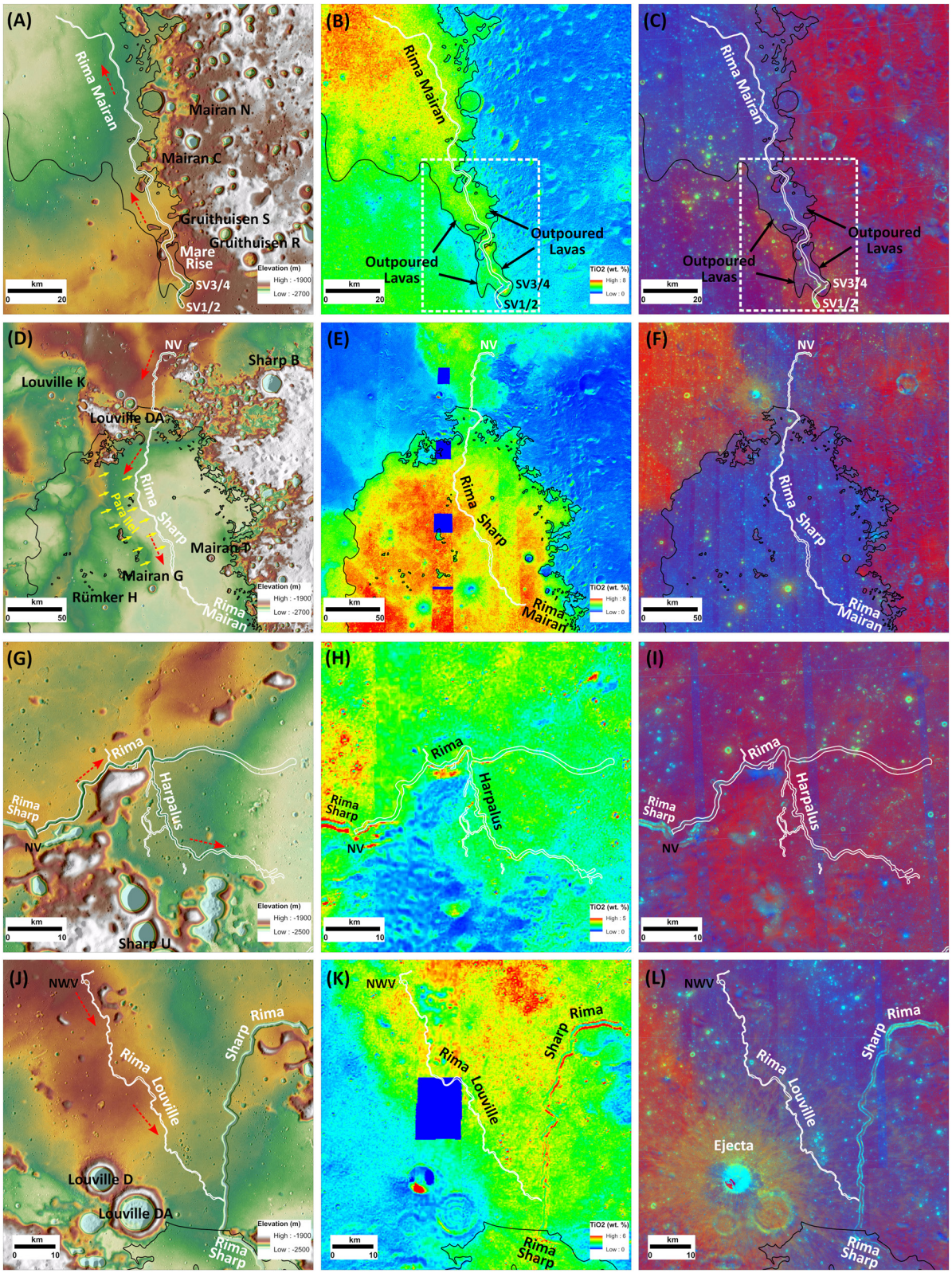

Figure 2. The elevation, TiO_2, and false-color maps of Rima Mairan (a–c), Rima Sharp (d–f), Rima Harpalus (g–i), and Rima Louville (j–l). The red arrows indicate the rille flow directions. The white-broken-line boxes indicate lavas outpoured from Rima Mairan, overlaying the low-Ti mare surface, maybe extending to the northwest of the outlined boxes.

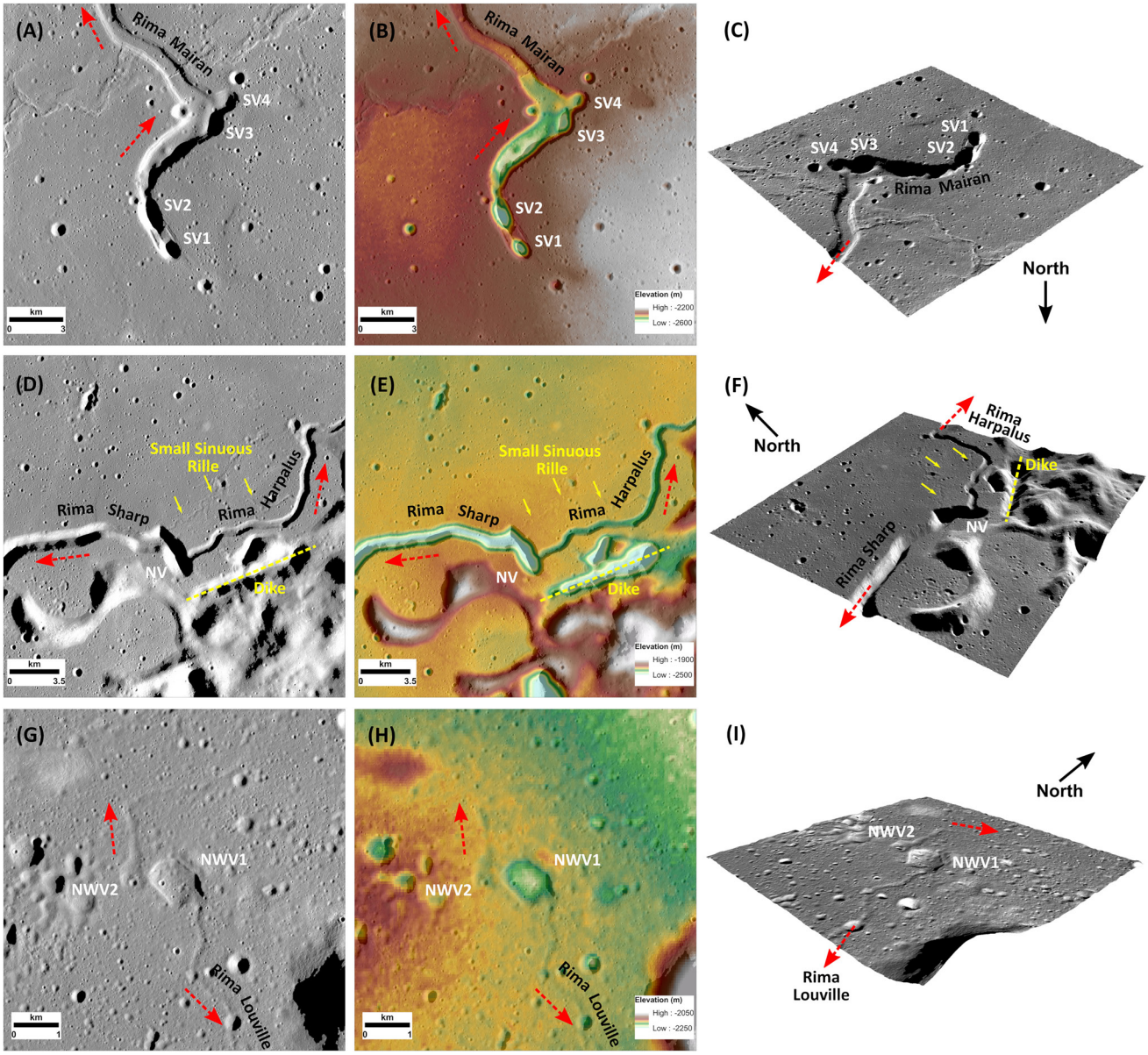

Figure 3. Source vents of Rima Mairan (a–c), Rima Sharp and Rima Harpalus (d–f), and Rima Louville (g–i).

Rima Mairan generally follows the regional slopes in a northwest direction (Figure 2a). High-Ti materials (~6–16 km-wide) are distributed in strips ~6–16 km-wide on both western and eastern sides of Rima Mairan close to the source vents (hashed box, Figures 2b and 2c) and overlie the Imbrian-aged low-Ti mare basalts (P40, Figure S1). Rima Mairan has a length of ~150 km, an average width of ~490 m, and a depth of ~46 m, before meeting Rima Sharp.

2.2. Rima Sharp

Rima Sharp originates from NV to the northwest of Sharp B crater (Figure 2d). NV is an ~320 m-deep, ~950 m-wide, and ~3,050 m-long elongated vent (NW-SE), which is ~14 m deeper than the Rima Sharp rille floor (Figure 3e). An ~8,900 m NE-SW linear depression is located southeast of NV (yellow-dashed line), but is not directly connected to NV.

The trend of Rima Sharp generally follows regional slopes, first west, then south across a highland valley near Louville DA crater, then to the center of Em4/P58 **(**Figure 2d**)**. No lava flows with compositions different from the young basalts are observed associated with the rille channel (Figures 2e and 2f), indicating either that lavas from the rille are coincidently the same as Em4/P58, or that Em4/P58 consists of products of the rille eruption. Rima Sharp has a length of ∼320 km, an average width of ∼920 m, and depth of ∼70 m, before meeting Rima Mairan.

2.3. Rima Harpalus and Rima Louville

Rima Harpalus also originates from NV, but flows east, in the direction opposite to Rima Sharp **(**Figure 2g**)**. Rima Harpalus, ∼76 km-long, averages ∼360 m width and ∼57 m depth, all values being smaller than Rima Sharp. The width of Rima Harpalus is generally constant from beginning to end, but the depth changes significantly (from ∼80 to ∼20 m).

Rima Louville originates from NWV northwest of Louville DA crater, and flows southeast before joining Rima Sharp (Figure 2j). NWV is composed of two separate irregular depressions, that is, NWV1 and NWV2 (Figures 3g–3i). NWV1 is the source vent of Rima Louville, while lavas from NWV2 extend north. The deepest point of NWV1 (∼43 m-deep, ∼570 m-wide, and ∼850 m-long) is ∼42 m lower than the rille floor. Rima Louville is the smallest rille (∼80 km-long, average width ∼190 m, depth ∼7 m) of all four rilles studied, and its width/depth vary little along the rille.

3. Chronology

3.1. Sinuous Rille Formation Sequence

We determined the relative ages of the major sinuous rilles in Em4/P58 using their cross-cutting relationships. Rima Harpalus, Rima Sharp, and another rille ("Small-Sinuous-Rille") share NV (Figures 3d–3f). Rima Sharp flows west; Rima Harpalus and Small-Sinuous-Rille flow east. Three pieces of evidence suggest that Rima Harpalus predates Rima Sharp, and that the Rima Harpalus channel was abandoned in the more extensive eruption phase of NV which produced Rima Sharp: (a) the floor of Rima Harpalus is ∼200 m higher than the floor of Rima Sharp in the vicinity of NV, (b) Rima Harpalus is much smaller than Rima Sharp, (c) there are no obvious lavas flowing from Rima Harpalus to Rima Sharp (yellow box, Figures S3a–S3c).

A small rille branch ("Small-Branch") of Rima Sharp occurs in the vicinity of highlands at ∼50.27°N, 46.08°W (Figures 4f and 4g, Figure S4). It first extends southeast after leaving the main branch, then turns southwest rejoining the main branch. Small-Branch is likely to be the product of an earlier eruption of Rima Sharp, because it cannot be traced back to any sources or other rilles. In earlier stages, a narrower Rima Sharp wound through highland obstacles, but as flow continued, it adopted a more direct SW course, abandoning the earlier narrower channel.

Rima Louville and Rima Sharp meet at ∼46.68°N, 50.65°W, ∼8 km to the north of the Em4/P58 boundary (Figure 2j). The Rima Louville floor is ∼185 m higher than that of Rima Sharp, and no lavas are observed draining onto the floor of Rima Sharp (yellow box, Figures S3d–S3f), indicating an older age of Rima Louville; the lavas from Rima Sharp may have been captured by the preexisting Rima Louville, and then buried and eroded it.

What is the temporal relationship between Rima Sharp and Rima Mairan, previously thought to be continuous? Based on our detailed mapping, we found that Rima Sharp and Rima Mairan meet at ∼40.40°N, 48.38°W in the southeast of Em4/P58 (Figures 4j–4l). At the meeting point, Rima Mairan is ∼250 m-wide and Rima Sharp is over three times wider (∼800 m). Rima Mairan (deep-blue lines) is observed entering the wider channel of Rima Sharp (light-blue lines) from southeast to northwest, clear evidence that Rima Mairan postdates Rima Sharp. Rima Sharp becomes shallower when encountering Rima Mairan, and finally becomes unidentifiable to the southeast of the meeting point, buried by the lavas from Rima Mairan. After entering Rima Sharp, Rima Mairan extends further into Rima Sharp from south to north, modifying inner features within it **(**Figures S5a–S5c**)**. These inner channels and levees are extensively developed in the southern part of Rima Sharp close to Rima Mairan (Figure S6). In addition, Rima Sharp is abnormally wide at ∼49.97°N, 41.92°W, with prominent inner features (Figures S5d–S5j), indicating that lavas from Rima

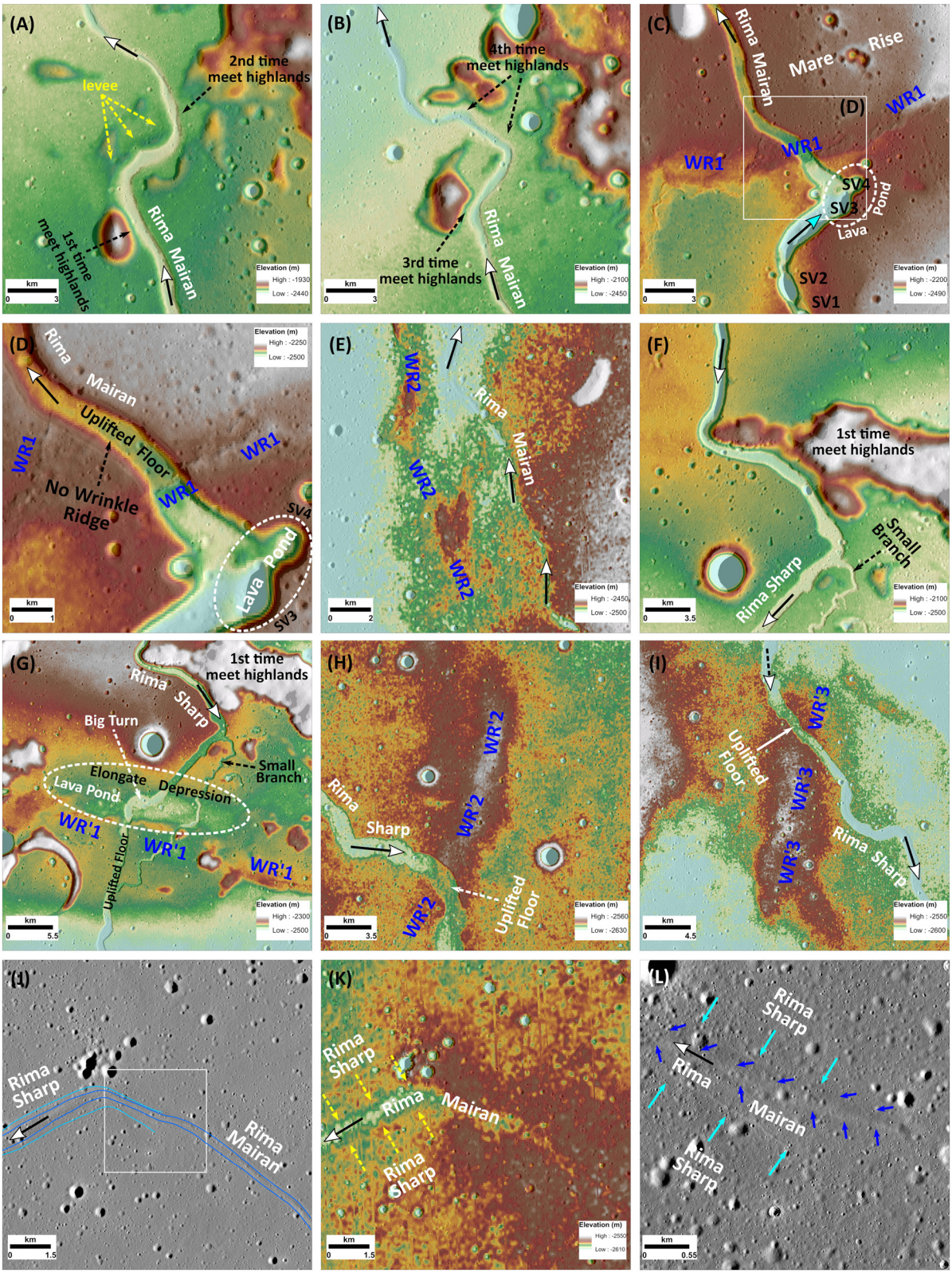

Figure 4. Rima Mairan encounters highlands (a–b) and wrinkle ridges (WR) (c–e). Rima Sharp encounters highlands (f) and WR (g–i). (j–l) Rima Mairan entered Rima Sharp, and produced a nested channel within Rima Sharp. The deep-blue lines and arrows represent Rima Mairan channels, and light-blue lines and arrows represent Rima Sharp channels. It can be seen that Rima Mairan entered Rima Sharp. Figure locations are shown in Figure S13.

Mairan may have ponded there, then eroded the surrounding mare surface before traveling further north. These observations indicate that Rima Sharp had formed and its associated lavas had solidified prior to the formation of Rima Mairan; then Rima Mairan was captured by Rima Sharp at their meeting point, scenarios for which are depicted in Figure S7.

3.2. CSFD Measurements

To further assess the stratigraphic relationships, we derived absolute model ages (AMAs) of the rille floors using crater size-frequency distribution measurements based on the Kaguya TC Morning Map (Text S1, Figure S8). Rima Louville ($2.20^{+0.52}_{-0.52}$ Ga) is the oldest, followed by Rima Sharp ($1.88^{+0.30}_{-0.30}$ Ga), and Rima Mairan is the youngest ($1.39^{+0.24}_{-0.24}$ Ga) (Figure S9), consistent with the stratigraphic relationships and supporting the rille capture interpretations. Rima Harpalus has not been dated because of extensive wall slumping and poor illumination; based on the analysis above, it appears to be older than Rima Sharp (Section 3.1).

Both the AMAs of Rima Sharp and Rima Mairan are close to the age of Em4/P58 ($1.53^{+0.027}_{-0.027}$ Ga, Qian, Xiao, Head, et al., 2021), although dating the rille floor has larger uncertainties. In addition, Rima Sharp in the north of Em4/P58 is slightly older than Rima Mairan in the south. Rima Sharp and Rima Mairan are surrounded by mare basalts with AMAs of ~1.6–1.7 and ~1.3–1.4 Ga, respectively (Figure 1b), supporting the conclusion that Em4/P58 formed by the eruption of lavas in association with rilles, further discussed in Section 4.3.

4. Discussion

Critical to further understanding of the rilles and their relationships to the emplacement of Em4/P58 is the nature of the topography and slopes that existed in the area of eruption and lava flooding. Clues to this information come from evidence for pre-existing topography at the time of unit emplacement and topography that formed subsequently.

4.1. Pre-Existing Topography

Besides the intrinsic fluid dynamic properties of the lava, lava flow emplacement (width, thickness, flow pathways, etc.) is also influenced by pre-existing topographic features (Chen et al., 2021; Minton et al., 2019). We find that rilles in the study area are controlled mainly by three types of pre-existing features, that is, highlands, older mare surfaces, and wrinkle ridges (WR).

Based on stratigraphic relationships, Rima Mairan is emplaced largely on the older Eratosthenian and Imbrian-aged mare units (Qian et al., 2018). Highlands (Figure 2a) to the NE consist of ejecta from the Imbrian-aged Iridum basin (~3.9 Ga; Ivanov et al., 2016), distinctly older than Rima Mairan (Section 3.2). Rima Mairan is influenced by pre-existing highlands in four locations before entering the majority of Em4/P58 (Figures 4a and 4b). Each encounter changes its width/depth dramatically, especially the second time (Figure 4a). Between the first and second encounter, the rille channel turns sharply to the northeast, where lava formed a levee on the left side. Following the second encounter, the width of Rima Mairan decreases by nearly half (from ~750 to 400 m), but the depth decreases slightly (from ~50 to 47 m).

We find evidence that Rima Mairan encountered preexisting WR four times (WR1 to WR4, Figure S10). First, a branch of WR1 extends to the rille floor, and the floor surface has been raised ~50 m (Figures 4c and 4d), indicating a younger age of WR1. However, just north of this branch, a much broader wrinkle ridge does not extend to the rille floor (black-dashed arrow, Figure 4d), indicating an older age of WR1, together suggesting that formation of WR1 was a continuous process, both predating and postdating Rima Mairan. SV3/SV4 are likely to be lava ponds accumulated behind WR1 in the early stage of emplacement by thermal erosion. When the lava from SV1/SV2 flowed toward the northeast, it was first hindered by proto-WR1, ponding locally and eroded down to produce SV3/SV4 (white-dashed circle, Figures 4c and 4d); then lava continued rising until a topographic pathway was found and northwesterly flow continued. Note that WR2/WR3 and the rille channel go north in parallel without crosscutting (WR2, Figure 4e; WR3, Figure S11a),

suggesting that proto-WR2/WR3 predate Rima Mairan and guided its flow. WR4 (Figure S11b), however, has no influence on the flow of rille, indicating a younger age of WR4.

Rima Sharp meets older highlands one time (Figure 4f), and this encounter not only changes the rille direction, but also decreases its depth from ~160 to ~50 m, while the width increases from ~700 to ~1,160 m. No clear evidence of lava overflowing around this point is observed.

Rima Sharp meets WR three times before terminating (WR′1 to WR′3, Figure S10). First, Rima Sharp makes a large angle behind WR′1 in an elongate depression that parallels WR′1, with a length of ~25 km and a width of ~4 km (white-dashed circle, Figure 4g); we interpret this to be the location of lava ponding. The proto-WR′1 appears to obstruct Rima Sharp, impeding its flow in the early stage and lava ponded locally behind this elongate depression. Lavas continued to accumulate until reaching a topographic gap, and then flowed southerly. WR′2/WR′3 are more subdued than WR′1, without clear interactions with the rille, therefore indicating that WR′2/WR′3 formed after Rima Sharp.

In summary, the formation of rilles and their associated lavas in Em4/P58 is significantly controlled by pre-existing features, including Imbrian-aged highlands, underlying mare units, and continuously evolving WR. The rille sources occur adjacent to highlands, which influenced their initial lava flow directions, but the vast majority of the rille's emplacement occur on the underlying mare units whose surfaces had already been deformed by pre-emplacement deformation and wrinkle ridge formation.

4.2. Post-Formation Tectonic Deformation

In order to assess the mode of emplacement of sinuous rilles and associated mare units, it is also important to deconvolve the tectonic modification that occurred subsequent to emplacement. Globally, the pre- and post-rille tectonic wrinkle ridge contractional deformation continued until as recently as ~1.2 Ga (Watters & Johnson, 2010), perhaps even to the present (Valantinas & Schultz, 2020). In the study area, WR are predominantly Imbrian-aged (~3.35 Ga) (Yue et al., 2017), predating all rilles (Section 3.2). As shown above, the early onset of wrinkle ridge formation suggests that the ridges are critical pre-existing topographic features controlling the formation of rilles (Section 4.1), even though the ridges were more subdued at the time of rille formation. We found abundant evidence that WR also deformed rilles after their formation.

WR1, cutting Rima Mairan, elevated the rille floor ~50 m to the north of SV3/4 (Figures 4c and 4d), and raised the mare surface above the source region. This phenomenon can only be explained by subsequent deformation, because the original flow of rille-forming lava will follow slopes and not extend from low to high elevations (Wilson & Head, 2017). WR′1, cutting Rima Sharp, also elevated the rille floor ~15 m after its formation, and deformed the surrounding mare (Figure 4g). The growth of WR1 and WR′1 thus both predate and postdate the rilles. For WR4, WR′2, and WR′3 (Figure S10), WR cut the middle, southwest, and northeast of rilles, leaving the remnants distributed on both sides of the rille channel (Figures 4h and 4i), suggesting that they are younger than the rilles. These WR are smaller than their Imbrian-aged counterparts and elevated the rille floor by <5 m.

Besides the WR, the regional load and subsidence of maria is another deformation factor (Solomon & Head, 1980). Em4/P58 (white-dashed circle, Figure S2) experienced ~100 m of subsidence after the loading of mare basalts: (a) Rima Sharp parallels contours (red arrows, Figures S2a and S2b), inconsistent with the rille formation theory (Wilson & Head, 2017), (b) gravity anomalies (Figures S2c and S2d) similar to those of lunar mascon basins (Neumann et al., 2015) imply loading, and (c) eastern Em4/P58 is located above the outer ring of the Imbrian basin, in which mare basalts may have preferentially accumulated (Spudis et al., 1988). Therefore, the current regional slope of rilles does not represent the original slope on which they formed. Following the formation of rilles, their elevations decreased as much as ~100 m due to mare subsidence, especially in the center of Em4/P58, and post-rille WR raised the rille floor a few tens of meters (Figure 4). This post-emplacement deformation must be subtracted when modeling the formation of the rilles and the emplacement of Em4/P58. The most likely topography at the time of rille formation was a relatively flat mare surface represented by earlier mare units, itself mildly deformed by WR.

4.3. Origin of Sinuous Rilles and Young Mare Basalts

Based on our reanalysis of the Rima Sharp/Mairan source vents, rille characteristics and stratigraphic relationships, and their relationship to Em4/P58, we call on the paradigm of basaltic magma ascent and eruption (see Figure S12 for the definition of eruption phases) outlined by Wilson and Head (2018) to reconstruct their emplacement (Figures 1c–1f). Following the short-lived Phase 1 as the dike reached the surface, Phase 2 involved a high-volume-flux Hawaiian eruptive phase as the magma degassed, forming a hemispherical pyroclastic fountain and attendant lava pond, the scale of which was dictated by the magma volatile content (Morgan et al., 2021). The initial high-flux stages of the eruption of both Rima Sharp and Rima Mairan (Phase 1) are likely to have involved the emplacement of sheet flows, rapidly flooding the surrounding topography. Phases 2 and 3 are predicted to involve the channelization of flow activity as the flow margins cooled, and the thermo-mechanical erosion of the rilles during the persistent and longer duration period of flow, with the rilles transporting lava to their distal ends until the termination of the eruption and solidification of the deposits. Source vent depths suggest eruption durations of 100–200 days (Wilson & Head, 2021). Because of the smaller size of Rima Mairan, its less extensive surrounding deposits, and its stratigraphic and age relationships, we interpreted the Rima Mairan eruption to have involved a much smaller total volume than Rima Sharp, and to have occurred after the emplacement and solidification of Rima Sharp and the majority of Em4/P58.

5. Conclusion

According to our analysis, we found that Rima Sharp, previously thought to be the longest lunar sinuous rille, is instead characterized by source vents at its beginning and end and is actually composed of two main rilles. The NV feeds several rilles, and the largest one, Rima Sharp, flows south into, and feeds Em4/P58. The SV begins at previously-thought rille terminus, and flows northward into Em4/P58. Neither sources appears to have substantial associated pyroclastic deposits. Rima Mairan postdates Rima Sharp, and flows into its southern end. Both source vents and rilles appear to be traversing and emptying into Em4/P58 and are thus likely to be the source of it. The composition of the basaltic lavas transported in both rilles appears very similar, despite their sources separation of ~350 km. Models for rille formation should account for these characteristics and relationships, and the nature of topography at the time of emplacement and produced subsequently.

Therefore, the CE-5 samples may have two different ages, potentially separated by several hundred million years, representing lavas from the two different rille sources, predominated lava from Rima Sharp, but with contributions from the younger Rima Mairan. Together these will form an unprecedented window into the petrogenesis of young mare basalts.

Data Availability Statement

LROC WAC data are from http://wms.lroc.asu.edu/lroc/view_rdr/WAC_GLOBAL, LROC WAC TiO_2 data are from http://wms.lroc.asu.edu/lroc/view_rdr/WAC_TIO2, SLDEM2015 data are from https://astrogeology.usgs.gov/search/map/Moon/LRO/LOLA/Lunar_LRO_LOLAKaguya_DEMmerge_60N60S_512ppd, Kaguya TC Morning Map and MI data are from https://darts.isas.jaxa.jp/planet/pdap/selene/index.html.en. Geological boundaries, geological features, CSFD ages in Figure 1b, and all the other data are from http://doi.org/10.5281/zenodo.4705974.

Acknowledgments
This research was funded by the National Key R&D Program of China (2020YFE0202100), the Pre-Research Project on Civil Aerospace Technologies (D020101, D020205), and the National Natural Science Foundation of China (41830214). Yuqi Qian was funded by the China Scholarship Council 201906410015. James W. Head gratefully acknowledges funding from the NASA Lunar Reconnaissance Orbiter Mission, Lunar Orbiter Laser Altimeter (LOLA) Experiment Team (Grant 80NSSC19K0605 from the National Aeronautics and Space Administration-Goddard).

References

Barker, M. K., Mazarico, E., Neumann, G. A., Zuber, M. T., Haruyama, J., & Smith, D. E. (2016). A new lunar digital elevation model from the lunar orbiter laser altimeter and SELENE terrain camera. *Icarus*, *273*, 346–355. https://doi.org/10.1016/j.icarus.2015.07.039

Carr, M. H. (1974). The role of lava erosion in the formation of lunar rilles and Martian channels. *Icarus*, *22*(1), 1–23. https://doi.org/10.1016/0019-1035(74)90162-6

Chen, Y., Head, J. W., Wilson, L., Kreslavsky, M. A., Liu, J., Ren, X., et al. (2021). The role of pre-existing topography in modulating lunar lava flow widths, depths, and channel structure. Paper presented at 52nd Lunar and Planetary Science Conference, Lunar and Planetary Institute. Retrieved from https://www.hou.usra.edu/meetings/lpsc2021/pdf/1818.pdf

Haruyama, J., Matsunaga, T., Matsunaga, T., Ohtake, M., Morota, T., Honda, C., et al. (2008). Global lunar-surface mapping experiment using the Lunar Imager/Spectrometer on SELENE. *Earth Planets and Space*, *60*(4), 243–255. https://doi.org/10.1186/BF03352788

Head, J. W., & Wilson, L. (2017). Generation, ascent and eruption of magma on the moon: New insights into source depths, magma supply, intrusions and effusive/explosive eruptions (Part 2: Predicted emplacement processes and observations). *Icarus*, *283*, 176–223. https://doi.org/10.1016/j.icarus.2016.05.031

Hiesinger, H., Head, J. W., Wolf, U., Jaumann, R., & Neukum, G. (2011). Ages and stratigraphy of lunar mare basalts: A synthesis. *Special Papers of the Geological Society of America*, *477*, 1–51. https://doi.org/10.1130/2011.2477(01)

Hulme, G. (1973). Turbulent lava flows and the formation of lunar sinuous rilles. *Modern Geology*, *4*, 107–117.

Hurwitz, D. M., Head, J. W., & Hiesinger, H. (2013). Lunar sinuous rilles: Distribution, characteristics, and implications for their origin. *Planetary and Space Science*, *79–80*(80), 1–38. https://doi.org/10.1016/j.pss.2012.10.019

Hurwitz, D. M., Head, J. W., Wilson, L., & Hiesinger, H. (2012). Origin of lunar sinuous rilles: Modeling effects of gravity, surface slope, and lava composition on erosion rates during the formation of Rima Prinz. *Journal of Geophysical Research*, *117*(E12), E00H14. https://doi.org/10.1029/2011je004000

Ivanov, M. A., Head, J. W., & Bystrov, A. (2016). The lunar gruithuisen silicic extrusive domes: Topographic configuration, morphology, ages, and internal structure. *Icarus*, *273*, 262–283. https://doi.org/10.1016/j.icarus.2015.12.015

Jolliff, B. L., Gillis, J. J., Haskin, L. A., Korotev, R. L., & Wieczorek, M. A. (2000). Major lunar crustal terranes: Surface expressions and crust-mantle origins. *Journal of Geophysical Research*, *105*(E2), 4197–4216. https://doi.org/10.1029/1999JE001103

Kodama, S., Ohtake, M., Yokota, Y., Iwasaki, A., Haruyama, J., Matsunaga, T., et al. (2010). Characterization of multiband imager aboard SELENE. *Space Science Reviews*, *154*, 79–102. https://doi.org/10.1007/s11214-010-9661-z

Liu, J., Zeng, X., Li, C., Ren, X., Yan, W., Tan, X., et al. (2021). Landing site selection and overview of china's lunar landing missions. *Space Science Reviews*, *217*(1), 6. https://doi.org/10.1007/s11214-020-00781-9

Minton, D. A., Fassett, C. I., Hirabayashi, M., Howl, B. A., & Richardson, J. E. (2019). The equilibrium size-frequency distribution of small craters reveals the effects of distal ejecta on lunar landscape morphology. *Icarus*, *326*, 63–87. https://doi.org/10.1016/j.icarus.2019.02.021

Morgan, C., Wilson, L., & Head, J. W. (2021). Formation and dispersal of pyroclasts on the moon: Indicators of lunar magma volatile contents. *Journal of Volcanology and Geothermal Research*, *413*, 107217. https://doi.org/10.1016/j.jvolgeores.2021.107217

Neumann, G. A., Zuber, M. T., Wieczorek, M. A., Head, J. W., Baker, D. M. H., Solomon, S. C., et al. (2015). Lunar impact basins revealed by gravity recovery and interior laboratory measurements. *Science Advances*, *1*(9), e1500852. https://doi.org/10.1126/sciadv.1500852

Oberbeck, V. R., Greeley, R., Morgan, R. B., & Lavas, M. J. (1971). Lunar rilles—A catalog and method of classification (NASA technical memorandum, NASA-TM-X-62088). https://doi.org/10.2172/4001896

Qian, Y., Xiao, L., Head, J. W., van der Bogert, C. H., Hiesinger, H., & Wilson, L. (2021). Young lunar mare basalts in the Chang'e-5 sample return region, northern oceanus procellarum. *Earth and Planetary Science Letters*, *555*, 116702. https://doi.org/10.1016/j.epsl.2020.116702

Qian, Y., Xiao, L., Wang, Q., Head, J. W., Yang, R., Kang, Y., et al. (2021). China's chang'e-5 landing site: Geology, stratigraphy, and provenance of materials. *Earth and Planetary Science Letters*, *561*, 116855. https://doi.org/10.1016/j.epsl.2021.116855

Qian, Y., Xiao, L., Zhao, S. Y., Zhao, J. N., Huang, J., Flahaut, J., et al. (2018). Geology and scientific significance of the Rümker region in Northern Oceanus Procellarum: China's Chang'E-5 landing region. *Journal of Geophysical Research: Planets*, *123*(6), 1407–1430. https://doi.org/10.1029/2018JE005595

Roberts, C. E., & Gregg, T. K. P. (2019). Rima Marius, the moon: Formation of lunar sinuous rilles by constructional and erosional processes. *Icarus*, *317*, 682–688. https://doi.org/10.1016/j.icarus.2018.02.033

Robinson, M. S., Brylow, S. M., Tschimmel, M., Humm, D., Lawrence, S. J., Thomas, P. C., et al. (2010). Lunar reconnaissance orbiter camera (LROC) instrument overview. *Space Science Reviews*, *150*, 81–124. https://doi.org/10.1007/s11214-010-9634-2

Sato, H., Robinson, M. S., Lawrence, S. J., Denevi, B. W., Hapke, B., Jolliff, B. L., & Hiesinger, H. (2017). Lunar mare TiO2 abundances estimated from UV/Vis reflectance. *Icarus*, *296*, 216–238. https://doi.org/10.1016/j.icarus.2017.06.013

Solomon, S. C., & Head, J. W. (1980). Lunar mascon basins: Lava filling, tectonics, and evolution of the lithosphere. *Reviews of Geophysics*, *18*(1), 107–141. https://doi.org/10.1029/RG018i001p00107

Spudis, P. D., Hawke, B. R., & Lucey, P. G. (1988). *Materials and formation of the Imbrium basin* (Vol. 18, pp. 155–168). Paper presented at 18th Lunar and Planetary Science Conference.

Valantinas, A., & Schultz, P. H. (2020). The origin of neotectonics on the lunar nearside. *Geology*, *48*(7), 649–653. https://doi.org/10.1130/G47202.1

Wang, J., Zhang, Y., Di, K., Chen, M., Duan, J., Kong, J., et al. (2021). Localization of the Chang'e-5 lander using radio-tracking and image-based methods. *Remote Sensing*, *13*, 590. https://doi.org/10.3390/rs13040590

Watters, T. R., & Johnson, C. L. (2010). Lunar tectonics. In T. R. Watters, & R. A. Schultz (Eds.), *Planetary tectonics* (pp. 121–182). Cambridge University Press.

Wilson, L., & Head, J. W. (2017). Generation, ascent and eruption of magma on the moon: New insights into source depths, magma supply, intrusions and effusive/explosive eruptions (Part 1: Theory). *Icarus*, *283*, 146–175. https://doi.org/10.1016/j.icarus.2015.12.039

Wilson, L., & Head, J. W. (2018). Controls on lunar basaltic volcanic eruption structure and morphology: Gas release patterns in sequential eruption hases. *Geophysical Research Letters*, *45*, 5852–5859. https://doi.org/10.1029/2018GL078327

Wilson, L., & Head, J. W. (2021). Lunar volcanic eruptions: Estimates of magma volatile contents, volumes, and eruption rates. Paper presented at 52nd Lunar and Planetary Science Conference, p. Abstract #1226.

Yue, Z., Michael, G. G., Di, K., & Liu, J. (2017). Global survey of lunar Wrinkle Ridge formation times. *Earth and Planetary Science Letters*, *477*, 14–20. https://doi.org/10.1016/j.epsl.2017.07.048

References From the Supporting Information

Chisenga, C., Yan, J., Zhao, J., Atekwana, E. A., & Steffen, R. (2020). Density structure of the Rümker region in the Northern Oceanus Procellarum: Implications for lunar volcanism and landing site selection for the Chang'E-5 mission. *Journal of Geophysical Research: Planets*, *125*(1), e2019JE005978. https://doi.org/10.1029/2019JE005978

Kneissl, T., van Gasselt, S., & Neukum, G. (2011). Map-projection-independent crater size-frequency determination in GIS environments-new software tool for ArcGIS. *Planetary and Space Science*, *59*(11), 1243–1254. https://doi.org/10.1016/j.pss.2010.03.015

Michael, G. G., Kneissl, T., & Neesemann, A. (2016). Planetary surface dating from crater size-frequency distribution measurements: Poisson timing analysis. *Icarus*, *277*, 279–285. https://doi.org/10.1016/j.icarus.2016.05.019

Michael, G. G., & Neukum, G. (2010). Planetary surface dating from crater size-frequency distribution measurements: Partial resurfacing events and statistical age uncertainty. *Earth and Planetary Science Letters*, *294*(3), 223–229. https://doi.org/10.1016/j.epsl.2009.12.041

Neukum, G. (1983). *Meteoritenbombardement und datierung planetarer oberflaechen*. University of Munich.

Neukum, G., Ivanov, B. A., & Hartmann, W. K. (2001). Cratering records in the inner solar system in relation to the lunar reference system. In R. Kallenbach, J. Geiss, & W. K. Hartmann (Eds.), *Chronology and evolution of mars* (pp. 55–86). Springer Netherlands. https://doi.org/10.1007/978-94-017-1035-0_3

Wieczorek, M. A., Neumann, G. A., Nimmo, F., Kiefer, W. S., Taylor, G. J., Melosh, H. J., et al. (2013). The crust of the moon as seen by GRAIL. *Science*, *339*(6120), 671–675. https://doi.org/10.1126/science.1231530

Zuber, M. T., Smith, D. E., Watkins, M. M., Asmar, S. W., Konopliv, A. S., Lemoine, F. G., et al. (2013). Gravity field of the moon from the gravity recovery and interior laboratory (GRAIL) mission. *Science*, *339*(6120), 668–671. https://doi.org/10.1126/science.1231507